Optics Letters

Reaching fiber-laser coherence in integrated photonics

Bohan Li,[1,†] Warren Jin,[2,†] Lue Wu,[1] Lin Chang,[2] Heming Wang,[1] Boqiang Shen,[1] Zhiquan Yuan,[1] Avi Feshali,[3] Mario Paniccia,[3] Kerry J. Vahala,[1,4] and John E. Bowers[2,5]

[1]T. J. Watson Laboratory of Applied Physics, California Institute of Technology, Pasadena, California 91125, USA
[2]ECE Department, University of California Santa Barbara, Santa Barbara, California 93106, USA
[3]Anello Photonics, Santa Clara, California 95054, USA
[4]e-mail: vahala@caltech.edu
[5]e-mail: jbowers@ucsb.edu

Received 5 August 2021; revised 24 September 2021; accepted 26 September 2021; posted 28 September 2021 (Doc. ID 439720); published 13 October 2021

We self-injection-lock a diode laser to a 1.41 m long, ultra-high Q integrated resonator. The hybrid integrated laser reaches a frequency noise floor of 0.006 Hz^2/Hz at 4 MHz offset, corresponding to a Lorentzian linewidth below 40 mHz—a record among semiconductor lasers. It also exhibits exceptional stability at low-offset frequencies, with frequency noise of 200 Hz^2/Hz at 100 Hz offset. Such performance, realized in a system comprised entirely of integrated photonic chips, marks a milestone in the development of integrated photonics; and, for the first time, to the best of our knowledge, exceeds the frequency noise performance of commercially available, high-performance fiber lasers.

https://doi.org/10.1364/OL.439720

Optical metrology applications such as optical atomic clocks, automotive LiDAR, bio-sensing, and microwave photonics are placing increasingly stringent demands on the spectral purity, form factor, and stability of light sources. These emerging applications require optical performance not currently available in silicon photonics plaforms from commercial foundries. Meanwhile, ultra-low-loss silicon nitride has emerged as a leading platform for realizing high-performance optical systems in a compact, affordable, and mass-manufacturable ways [1,2]. Integrated resonators with 260 M Q factor and bend radius below 1 mm [3] and on-chip delay lines over 20 m in length [4] have been fabricated on 200 mm wafers in complementary metal-oxide semiconductor (CMOS) foundries. This suggests that Q factors over 100 M, long the exclusive domain of academic research, may soon become accessible to real-world applications.

Recent advances have revealed a pathway towards ultra-narrow linewidth on-a-chip by self-injection-locking (SIL) integrated lasers to ultra-high Q microresonators [3,5,6]. Compared to other means of laser stabilization, such as Pound–Drever–Hall locking of a laser to a reference cavity, SIL is well suited to integrated photonics due to its simplicity. Coupling a diode laser chip to a silicon nitride chip in a hybrid [3,5,7–9] or heterogeneous [6] integration scheme stabilizes the laser without extraneous hardware such as electronic control circuitry, modulators, or isolators. In SIL, surface and bulk inhomogeneities in the resonator lead to backscattering. When the laser frequency is aligned sufficiently close to a resonance frequency, the optical field reflected from within the resonator provides feedback to spontaneously align the laser to the resonance, dramatically reducing the laser linewidth [10–13]. The frequency noise (FN) reduction is proportional to the resonator Q factor squared [14], such that for sufficiently high Q factor the laser linewidth reaches the thermodynamic limit imposed by microscopic thermal fluctuations within the resonator [15]. In this work, we probe the limit imposed by this thermorefractive noise (TRN) in ultra-low-loss silicon nitride waveguides by fabricating large-mode-volume spiral resonators [16]. Through SIL of a laser diode, these devices demonstrate FN at or beyond the level of high-performance fiber lasers.

To achieve large-mode volume in a compact footprint, we design spiraled resonators [16] in an ultra-low-loss integrated photonic platform [3,17] featuring a 100 nm thick silicon nitride core, 2.2 μm thick tetraethyl-orthosilicate (TEOS) -based silicon dioxide top cladding, and 14.5 μm thick thermally oxidized silicon dioxide bottom cladding. The devices [pictured in Fig. 1(a)] were fabricated on 200 mm silicon wafers in a CMOS foundry [3]. Each resonator is drawn from two identical Archimedes spirals [18] with 40 μm pitch and minimum bend radius of 2 mm. The two spirals share a common center of curvature and are interleaved by rotating one spiral by 180° with respect to the other. The resonator is formed by linking interior and exterior spiral endpoints with adiabatically curved transitions [19] with 0.9 mm minimum bend radius, drawn to precisely match the direction and curvature with the spiral endpoints. Each adiabatic transition maintains 2.8 μm single-mode-waveguide width to prevent coupling to higher-order modes, while the waveguides widen to 10 μm waveguide width within the Archimedes spirals to minimize propagation loss. Two couplers are drawn along the outermost loop of the spiral

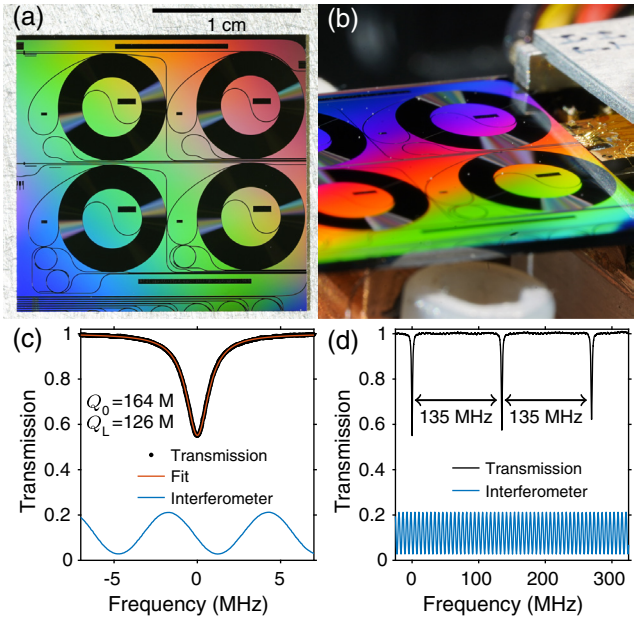

Fig. 1. (a) Photograph of 1.41 m round-trip-length spiral resonators. Each resonator occupies a 9.2 mm × 7.2 mm footprint. The chip features four independent, identical resonators, each designed with a different coupling strength. (b) Photograph of self-injection-locking (SIL) setup. (c) The transmission spectrum of a 1.41 m resonator with the measured intrinsic ($Q_0 = 164$) and loaded ($Q_L = 125.9 \pm 0.2$) Q-factor values indicated. An average propagation loss of 0.17 dB/m within the resonator is implied by Q_0. Intrinsic Q factor is calculated assuming the coupling rate of the drop port is 0.7 of the through port, inferred from the design. (d) Transmission spectrum showing FSR of 135 MHz (134.73 ± 0.01 MHz) at 1551 nm.

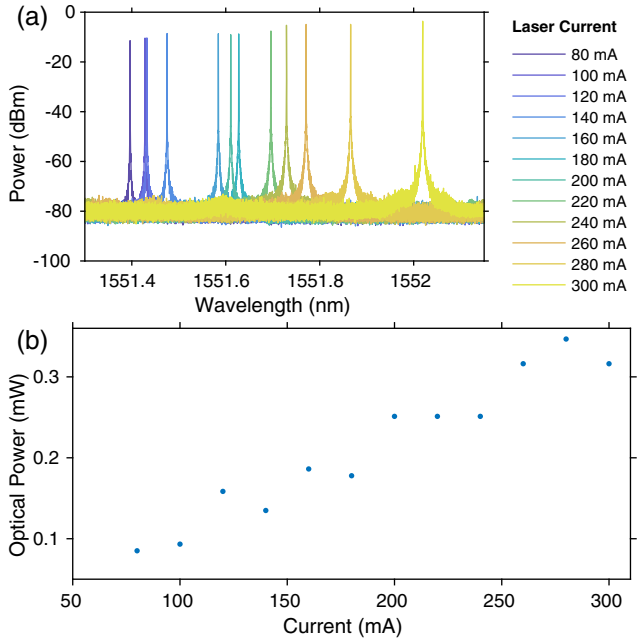

Fig. 2. (a) Single-mode lasing with large side-mode suppression ratio (SMSR) and (b) output power taken from the drop port of the SIL device (from a different scan) are shown for the 1.41 m long resonator at a series of pumping currents to the distributed feedback (DFB) laser. The data in (a) are collected using an optical spectrum analyzer (OSA) with 5 MHz resolution bandwidth (Apex AP2051A) in order to confirm single-mode operation.

to allow the SIL laser output to be taken from the drop port and thereby filter out high-offset FN [3]. Resonators featuring round-trip length of 1.41 m [shown in Fig. 1(a)] and 0.312 m length (not pictured) were fabricated, with a free spectral range (FSR) of 135 MHz and 610 MHz, respectively. The typical setup for SIL is shown in Fig. 1(b). A commercial distributed-feedback (DFB) laser is butt-coupled to the spiral resonator using a six-axis alignment stage and is powered by an ultra-low-noise current source (ILX Lightwave LDX-3620B). Intrinsic and loaded Q factors as well as the FSR are measured for each resonator using a tunable laser calibrated by a fiber interferometer, as illustrated for the 1.41 m resonator in Figs. 1(c) and 1(d). Further details regarding the SIL and measurement setups are provided in Appendix A.

As shown in Fig. 2(a), single-mode lasing with large side-mode suppression ratio (SMSR) can be achieved over a wide range of pumping currents. Typical output power, collected from the drop port of the resonator, for the same range of pumping current, is shown in Fig. 2(b). At each pumping condition, the air gap between the chips is adjusted to control the feedback phase [10] to achieve single-mode lasing. Moreover, at any given pumping current, single-mode lasing can be observed at multiple distinct wavelengths depending on feedback phase. As a result, the wavelengths in Fig. 2(a) and power in Fig. 2(b) do not increase monotonically with the driving current, as they would in a free-running DFB laser. We note that below 80 mA single-mode lasing could not be achieved for any feedback phase. Details of the single-mode lasing condition in the DFB-spiral system are under further study. Although the laser chip is mounted on a thermoelectric cooler, the spiral resonator is not temperature stabilized. Also, the air gap is not feedback stabilized. We believe that drift in the feedback phase and ambient temperature contribute to occasional mode hops between adjacent resonances of the resonator that were observed to occur on a time scale of approximately 1 h. These factors could be addressed by packaging the device to improve thermal and mechanical stability [20]. In a packaged device, as the gap between chips would no longer be adjustable, a resistive heater [6] placed between the resonator and laser could be used instead to tune the feedback phase by the thermo-optic effect.

The FN of the DFB laser self-injection-locked to the spiral resonators is shown in Fig. 3(a). A commercial FN tester (OE4000) is used to measure FN below 10 kHz offset frequency. We combine this with a self-heterodyne cross-correlation method [3,21] with higher sensitivity at offset frequency above 10 kHz. To explore the dependence on mode volume, we also measure the FN of the DFB laser self-injection-locked to 30, 10, and 5 GHz FSR resonators studied in prior work [3]. The FN of these devices rises at high-offset frequency (>2 MHz) due to their through-port configuration, as the FN reduction factor decreases for offset frequency beyond the resonator's resonance bandwidth [11]. However, the spiral resonators exhibit flat FN reduction factor at high-offset frequency [3] due to their drop-port configuration. We note that the noise spectrum for the FSR = 135 MHz spiral device rises for offset frequencies above 4 MHz due to reaching the measurement-limited noise

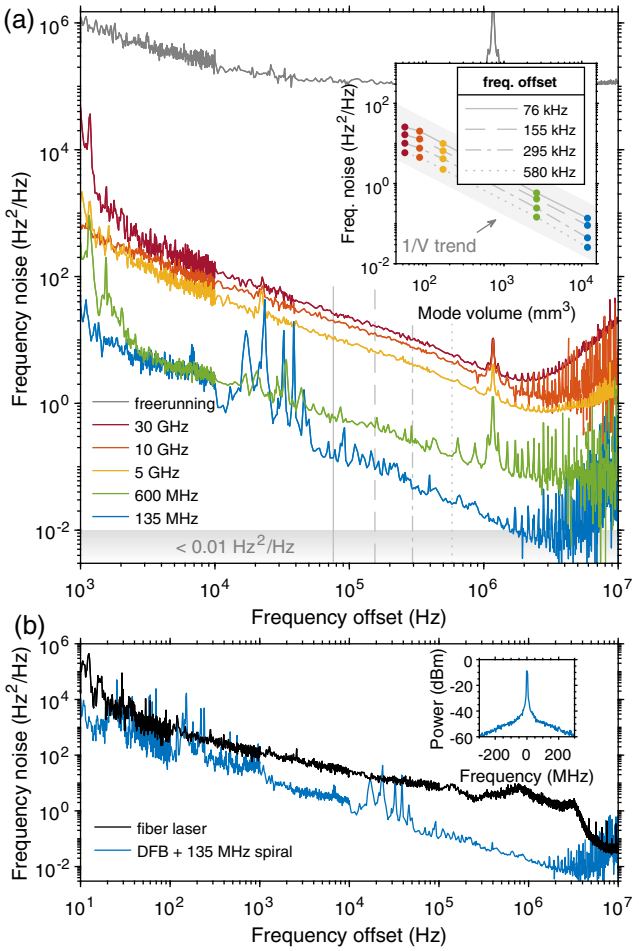

Fig. 3. (a) Single-sideband frequency noise (FN) spectra of the DFB laser in free-running state, as well as in the SIL mode to resonators of various FSR. Vertical lines indicate the frequency offsets selected in the inset. Inset: FN versus mode volume at offset frequencies selected to avoid noise spurs and reveal the TRN floor. (b) FN comparison of a high-performance fiber laser to the SIL DFB laser using a 135 MHz spiral resonator. Inset: high-resolution optical spectrum of SIL DFB laser.

floor (see Appendix A). FN below 10 kHz offset is strongly influenced by environmental perturbations and could be reduced by packaging, as discussed above. In the 10 kHz to 1 MHz range, we expect the FN to be dominated by thermorefractive contributions. In the inset, FN is plotted versus resonator mode volume, V, at selected offset frequencies. The data show strong agreement with the expected $1/V$ trend of TRN [15].

As shown in Fig. 3(b), the FN of the DFB self-injection-locked to the 135 MHz spiral is comparable to or better than a high-performance fiber laser (Orbits Ethernal) over a wide range of offset frequencies. At high-offset frequency, it outperforms the fiber laser by over an order of magnitude, reaching 0.006 Hz^2/Hz at 4 MHz, corresponding to Lorentzian linewidth [3] below 40 mHz. Remarkably, the hybrid laser exhibits stability comparable to the fiber laser in the 100 Hz to 10 kHz frequency offset range as well, with a FN level of 200 Hz^2/Hz at 100 Hz offset. In all configurations, we confirm single-mode operation of the SIL laser [Fig. 3(b) inset] using a high-resolution (5 MHz resolution bandwidth) optical spectrum analyzer. We note that the noise spurs around 1 MHz offset, present in certain measurements, come from the pump current source and are absent when using a different current source of the same model.

Finally, we compare this work with previous literature on narrow-linewidth integrated lasers. The Lorentzian (high-offset white FN) linewidth is less than 0.04 Hz in this work, limited by the measurement noise floor. This substantially improves upon the 1.2 Hz linewidth in [3], the 25 Hz linewidth in [7], and also surpasses the 0.1 Hz linewidth using non-planar crystalline resonators [20], achieved by SIL. The current result is also much smaller than the 13 kHz [22] and 40 Hz linewidths [23] demonstrated for silicon-nitride-external-cavity hybrid integrated lasers.

In conclusion, we self-injection-locked a DFB laser to a large-mode-volume spiral resonator to reduce TRN. The resulting device has outstanding FN characteristics that are comparable to or exceed that of a high-performance fiber laser. Further improvements in wafer-scale heterogeneous integration may soon unite the laser and ultra-high Q resonator on a single substrate [6], enabling the production of mass-manufactured laser sources with fiber-laser-equivalent coherence on a chip.

APPENDIX A: MEASUREMENT DETAILS

We use a high-power continuous wave (CW) 1550 nm DFB laser diode chip manufactured by Shenzhen PhotonX Technology Co. Ltd. The free-running DFB laser exhibits a lasing threshold of 15 mA, wavelength tunability of approximately 1 nm over a range of pump current up to 300 mA, and outputs 80 mW optical power for 250 mA pump current. The DFB laser and lensed fiber are coupled to the resonator using precision alignment stages (Thorlabs Nanomax 300 and 600). The total coupling loss, comprising coupling of the DFB laser to the on-chip waveguide and coupling from the on-chip waveguide to lensed fiber, is approximately 10 dB, while the insertion loss of the spiral resonator to its drop port is modeled to be 13 dB, due to the resonator being undercoupled.

Details of the FN measurement method are provided in [3,21]. Detectors used in the FN setup are a pair of Thorlabs PDB470C balanced photodetectors, and a Keysight DSOS104A oscilloscope is used to record the data. The measurement-limited noise floor, reached by the FSR = 135 MHz device in Fig. 3, is determined by the combination of the intrinsic photodetector noise and the noise suppression factor of the cross-correlation technique on the photodetector noise (limited to 15 dB by the 50 ms time duration of data collection [21]). The resulting noise floor scales with offset frequency, f, as f^2. All FN measurements in Fig. 3 are taken with pump currents in the range from 240 to 250 mA, with the laser wavelength around 1551 nm. However, the FN spectra shown in Fig. 3 are typical of the SIL device for pump currents in the 100 to 300 mA range, which has been verified experimentally but not included in this paper.

Funding. DARPA LUMOS (HR001-20-2-0044); Anello Photonics.

Acknowledgment. The authors thank Yaakov Shevy and Reginald Lee from Orbits Lightwave for supplying the EthernalTM fiber laser.

Disclosures. The authors declare no conflicts of interest.

Data Availability. Data underlying the results presented in this paper are not publicly available at this time but may be obtained from the authors upon reasonable request.

[†]These authors contributed equally to this Letter.

REFERENCES

1. D. J. Blumenthal, R. Heideman, D. Geuzebroek, A. Leinse, and C. Roeloffzen, Proc. IEEE **106**, 2209 (2018).
2. J. Liu, G. Huang, R. N. Wang, J. He, A. S. Raja, T. Liu, N. J. Engelsen, and T. J. Kippenberg, Nat. Commun. **12**, 2236 (2021).
3. W. Jin, Q.-F. Yang, L. Chang, B. Shen, H. Wang, M. A. Leal, L. Wu, M. Gao, A. Feshali, M. Paniccia, K. J. Vahala, and J. E. Bowers, Nat. Photonics **15**, 346 (2021).
4. W. Jin, A. Feshali, M. Paniccia, and J. Bowers, Opt. Lett. **46**, 2984 (2021).
5. B. Shen, L. Chang, J. Liu, H. Wang, Q.-F. Yang, C. Xiang, R. N. Wang, J. He, T. Liu, W. Xie, J. Guo, D. Kinghorn, L. Wu, Q.-X. Ji, T. J. Kippenberg, K. J. Vahala, and J. E. Bowers, Nature **582**, 365 (2020).
6. C. Xiang, J. Liu, J. Guo, L. Chang, R. N. Wang, W. Weng, J. Peters, W. Xie, Z. Zhang, J. Riemensberger, J. Selvidge, T. J. Kippenberg, and J. E. Bowers, Science **373**, 99 (2021).
7. G. Lihachev, J. Riemensberger, W. Weng, J. Liu, H. Tian, A. Siddharth, V. Snigirev, R. N. Wang, J. He, S. A. Bhave, and T. J. Kippenberg, "Ultralow-noise frequency-agile photonic integrated lasers," arXiv:2104.02990 (2021).
8. R. Oldenbeuving, E. Klein, H. L. Offerhaus, C. J. Lee, H. Song, and K. J. Boller, Laser Phys. Lett. **10**, 015804 (2012).
9. Y. Fan, J. P. Epping, R. M. Oldenbeuving, C. G. Roeloffzen, M. Hoekman, R. Dekker, R. G. Heideman, P. J. van der Slot, and K.-J. Boller, IEEE Photon. J. **8**, 1505111 (2016).
10. B. Dahmani, L. Hollberg, and R. Drullinger, Opt. Lett. **12**, 876 (1987).
11. D. R. Hjelme, A. R. Mickelson, and R. G. Beausoleil, IEEE J. Quantum Electron. **27**, 352 (1991).
12. N. Kondratiev, V. Lobanov, A. Cherenkov, A. Voloshin, N. Pavlov, S. Koptyaev, and M. Gorodetsky, Opt. Express **25**, 28167 (2017).
13. A. B. Matsko, A. A. Savchenkov, N. Yu, and L. Maleki, J. Opt. Soc. Am. B **24**, 1324 (2007).
14. H. Li and N. Abraham, IEEE J. Quantum Electron. **25**, 1782 (1989).
15. M. L. Gorodetsky and I. S. Grudinin, J. Opt. Soc. Am. B **21**, 697 (2004).
16. H. Lee, M.-G. Suh, T. Chen, J. Li, S. A. Diddams, and K. J. Vahala, Nat. Commun. **4**, 2468 (2013).
17. J. F. Bauters, M. J. Heck, D. John, D. Dai, M.-C. Tien, J. S. Barton, A. Leinse, R. G. Heideman, D. J. Blumenthal, and J. E. Bowers, Opt. Express **19**, 3163 (2011).
18. T. Chen, H. Lee, and K. J. Vahala, Opt. Express **22**, 5196 (2014).
19. F. Ladouceur and E. Labeye, J. Lightwave Technol. **13**, 481 (1995).
20. W. Liang, V. Ilchenko, D. Eliyahu, A. Savchenkov, A. Matsko, D. Seidel, and L. Maleki, Nat. Commun. **6**, 7371 (2015).
21. H. Wang, L. Wu, Z. Yuan, and K. Vahala, "Towards milli-hertz laser frequency noise on a chip," arXiv:2010.09248 (2020).
22. B. Stern, X. Ji, A. Dutt, and M. Lipson, Opt. Lett. **42**, 4541 (2017).
23. Y. Fan, A. van Rees, P. J. Van der Slot, J. Mak, R. M. Oldenbeuving, M. Hoekman, D. Geskus, C. G. Roeloffzen, and K.-J. Boller, Opt. Express **28**, 21713 (2020).